

# Metamagnetism and Weak Ferromagnetism in Nickel (II) oxalate crystals

E Romero<sup>1</sup>, M E Mendoza<sup>1</sup>, and R Escudero<sup>2</sup>

<sup>1</sup>*Instituto de Física, Benemérita Universidad Autónoma de Puebla,  
Apartado Postal J-48, Puebla 72570, México and*

<sup>2</sup>*Instituto de Investigaciones en Materiales, Universidad Nacional Autónoma de México,  
Apartado Postal 70-360, México DF 04510, México\**

(Dated: November 27, 2024)

Microcrystals of orthorhombic nickel (II) oxalate dihydrate were synthesized through a precipitation reaction of aqueous solutions of nickel chloride and oxalic acid. Magnetic susceptibility exhibits a sharp peak at 3.3 K and a broad rounded maximum near 43 K. We associated the lower maximum with a metamagnetic transition that occurs when the magnetic field is about  $\geq 3.5$  T. The maximum at 43 K is the typical of 1D antiferromagnets, whereas weak ferromagnetism behavior was observed in the range of 3.3 to 43 K.

PACS numbers: 75.10.Pq; 75.30.Et; 75.50.Xx

## I. INTRODUCTION

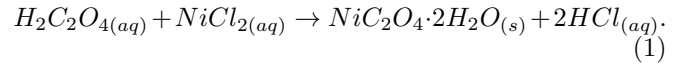
It has been shown, theoretically and experimentally, that if a critical magnetic field  $H$  is applied along the crystalline anisotropy axis of an antiferromagnet (AF), there occurs a nearly  $90^\circ$  rotation of the sublattice vectors. An antiferromagnetic material with such a behavior is known as a metamagnet [1, 2]. This behavior has been observed in compounds like:  $CuCl_2 \cdot 2H_2O$  [3],  $FePt_3$ ,  $YCO$ ,  $TiBe_2$  [4], and  $Ni(C_2O_4)(bpy)$ , where  $bpy = 4,4' - bipyridine(C_{10}H_8N_2)$  [5], when applying high magnetic fields (from 10 to 50 T). The type of ordering in  $Fe(C_2O_4)(bpy)$ , and  $Co(C_2O_4)(bpy)$  is also antiferromagnetic but with canted spins. This uncompensated antiferromagnetism produces weak ferromagnetism (WF). Recently, investigations in the quasi-one-dimensional magnetic compound  $\beta - CoC_2O_4 \cdot 2H_2O$  [6] revealed that the intra and interchain magnetic interactions tilt the spins, distorting the antiferromagnetic order and producing the WF.

The orthorhombic  $\beta$ -phase of nickel oxalate dihydrate belongs to the space group  $Cccm$  with cell parameters  $a = 11.842(2)$  Å,  $b = 5.345(1)$  Å, and  $c = 15.716(2)$  Å [7]. In this structure, oxalate bridges link  $Ni^{2+}$  ions chains along the  $b$  direction [8–11] and they mediate a dominant antiferromagnetic intrachain superexchange interaction [12]. Its molar susceptibility data exhibits the broad rounded maximum typical of 1D antiferromagnets with  $T_{max} \sim 41$  K [13].

In this paper we report results on the synthesis, crystal structure, and magnetic measurements of the orthorhombic  $\beta - NiC_2O_4 \cdot 2H_2O$  microcrystals. We determined by isothermal  $M - H$  measurements, from 2 to 80 K, that this phase exhibits weak ferromagnetism in the range of 3.3 to 43 K. At low temperature a metamagnetic order is observed under an applied field  $\geq 3.5$  T, in  $\chi - T$  measurements.

## II. EXPERIMENTAL METHODS

The synthesis of  $\beta -$  nickel oxalate dihydrate under nitrogen atmosphere was carried out by precipitation reaction of aqueous solutions of nickel (II), chloride 0.1 M (Aesar, 99.9995%) and oxalic acid 0.00625 M (Baker,  $\geq 99.9\%$ ), following the chemical equation,



The precipitates were filtered and dried at room temperature. Morphological analyses were performed with a scanning electron microscope (SEM) Cambridge-Leica Stereoscan 440. Powder X-ray diffraction patterns were acquired using a Siemens D5000 diffractometer operating in the Bragg-Brentano geometry with  $\lambda(Cu-K\alpha) = 1.541$  Å, and  $2\theta$  scan from  $10 - 70^\circ$ , and step size of  $0.02^\circ$ . Thermogravimetric (TG) and differential thermal analysis (DTA) curves were obtained in a SDT-TA Instruments model 2960 in air atmosphere with a heating rate of  $5^\circ C/min$ , from room temperature up to  $600^\circ C$ . Magnetization measurements were done with a Quantum Design MPMS SQUID magnetometer, MPMS-5. Zero Field Cooling (ZFC) and Field Cooling (FC) cycles were performed at magnetic field intensities from 0.01 T to 5.00 T, in the range 2 up to 250 K. Isothermal magnetization measurements  $M(H)$  were obtained from 2 K - 80 K. The diamagnetic contribution calculated from Pascal's constants [14] was  $\chi_{Di} = -72 \cdot 10^{-6} \text{ cm}^3/\text{mol}$ .

## III. RESULTS AND DISCUSSION

### A. Synthesis

Prismatic green microcrystals of nickel oxalate dihydrate were obtained after eight days of growth in nitrogen atmosphere. Figure 1 presents a SEM micrograph of the crystals with average length size (L) and diameter (D) of 1.47 and 0.65  $\mu\text{m}$ , respectively. Chemical analysis by

\* Author to whom correspondence should be addressed. ER, email address: evarotel@gmail.com

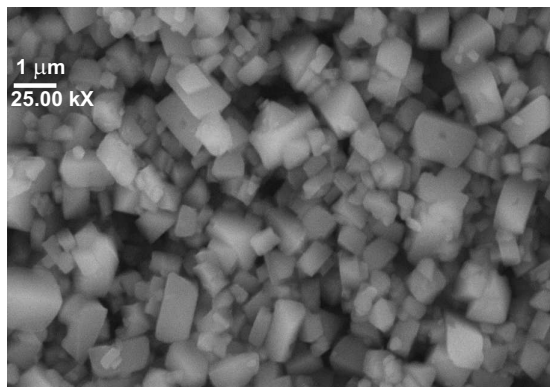


FIG. 1. SEM micrographs of  $\beta$  nickel oxalate dihydrate shows prismatic-like shapes. Average length size (L) and diameter (D) were 1.47 and 0.65  $\mu\text{m}$ , respectively.

digestion/ICP-OEP, combustion/TCD/IR-detection and Pyrolysis/IR-detection, gave the composition in weight of 31.82 % in nickel, 13.21 % in carbon, 2.48 % in hydrogen and 51.00 % in oxygen.

### B. Structural characterization

Figure 2a displays the XRD powder diffraction pattern of  $\text{NiC}_2\text{O}_4 \cdot 2\text{H}_2\text{O}$  (blue pattern); it is in good agreement with the reported (red lines) for the orthorhombic  $\beta$ -phase of cobalt oxalate dihydrate (JCPDS file: 25-0250). This figure also shows the Rietveld profile fit (red pattern). In figure 2b the difference pattern (red) obtained by using the Win-Rietveld software [15]. Background was estimated by linear interpolation and the peak shape was modeled by Pseudo-Voigt function. Unit cell parameters were  $a = 11.842 \text{ \AA}$ ,  $b = 5.345 \text{ \AA}$ , and  $c = 15.716 \text{ \AA}$  [7]. The atomic positions were the reported by Deyrieux et al., for iron-oxalate [10]; i.e.  $4\text{Co}(\frac{1}{4}, \frac{1}{4}, 0)$ ,  $4\text{Co}(0, 0, \frac{1}{4})$ ,  $8\text{C}_{oxalate}(\frac{1}{4}, \frac{1}{4}, 0.042)$ ,  $8\text{C}_{oxalate}(0, \frac{1}{2}, 0.042)$ ,  $16\text{O}_{oxalate}(\frac{1}{4}, 0.0941, 0.089)$ ,  $16\text{O}_{oxalate}(0, 0.691, 0.339)$ ,  $8\text{O}_{water}(0.423, \frac{1}{4}, 0)$ , and  $8\text{O}_{water}(0.173, 0, \frac{1}{4})$ . The weighted profile and expected residuals factors obtained in the refinement were  $R_{wp} = 32.52$ , and  $R_{exp} = 13.52$ .

It must be noticed that some low intensity calculated peaks were absent in the experimental pattern (black peaks in figure 2a. this could be due to the method of preparation.

Refined cell parameters determined for the orthorhombic phase of Ni-oxalate sample were  $a = 11.759(3) \text{ \AA}$ ,  $b = 5.327(1) \text{ \AA}$ , and  $c = 15.654(4) \text{ \AA}$ . Schematic representation of the unit cell is shown in figure 3. There are two non equivalent positions for nickel ions, designed as Ni1 and Ni2, each nickel ion is shifted one respect to of other by a translation vector  $(\frac{1}{2}, \frac{1}{2}, 0)$ .

Finally, the coherent diffraction size ( $D$ ) for the sample crystallites was calculated with the Scherrer equation [16]

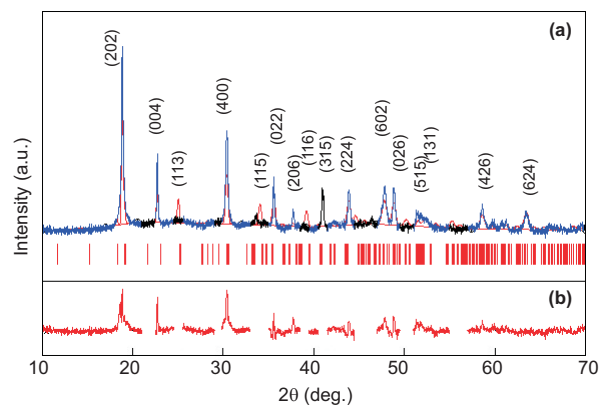


FIG. 2. (Color online) (a) X-ray powder diffraction pattern of nickel oxalate dihydrated (blue), peaks absent (black), Rietveld calculated pattern (red) and Miller index (red lines) reported for the orthorhombic  $C_{ccm}$  phase (JCPDS file: 25 - 0250). (b) Difference pattern (red).

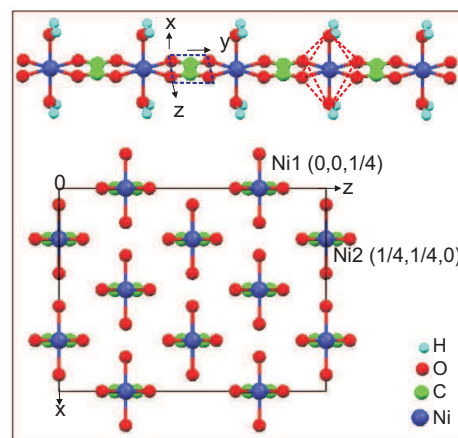


FIG. 3. (Color online) Ni-oxalate unit cell of the orthorhombic  $\beta$ -phase of JCPDS file 25-0250, space group  $C_{ccm}$ . The eight nickel atoms are located in two non-equivalent positions designed as Ni1 and Ni2.

using the (202) peak, the calculated value was 21.4 nm.

### C. Thermal analysis

Figure 4 shows the TG and DTA curves of  $\text{NiC}_2\text{O}_4 \cdot 2\text{H}_2\text{O}$ . Two steps of weight loss were observed. The first one ending at 188  $^\circ\text{C}$  and the second one finishing at 318  $^\circ\text{C}$ . In the first step the weight loss of 19.93 % corresponds to the loss of two water molecules, which agrees with the theoretical value of 19.73 %. DTA curve associated with this process shows an endothermic peak at 188  $^\circ\text{C}$ . The dehydration reaction is:



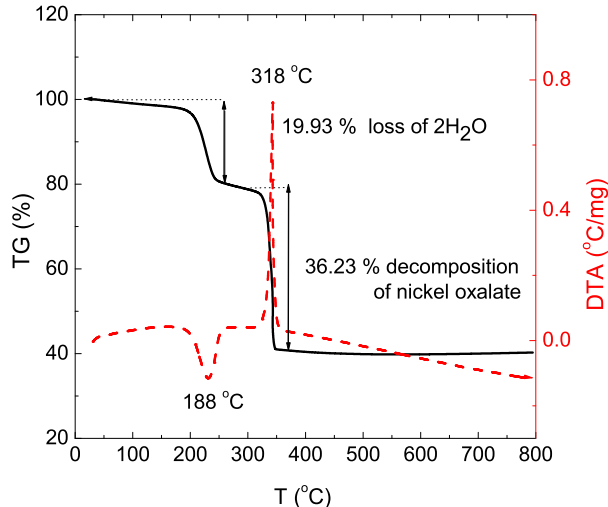


FIG. 4. (Color online) The TG (solid line) / DTA (dash line) curves for  $NiC_2O_4 \cdot 2H_2O$  at  $5^\circ C/min$  heating rate.

The weight loss about 36.23 % in the second step may be associated to the decomposition to the anhydrous nickel oxalate to nickel oxide, this agrees with the theoretical value of 39.85 % [17, 18]. The corresponding DTA curve shows an exothermic peak, at  $T = 318^\circ C$ . The decomposition reaction in this step can be written as



#### D. Magnetic measurements

The molar susceptibility  $\chi(T)$ , for the sample is shown in figure 5. It was measured by applying magnetic fields of 0.01 T, 0.50 T, and 5.00 T in both ZFC, and FC modes. The main panel shows two well defined maxima in the susceptibility at 3.3 K and 43 K. We also observed changes in the susceptibility at 3.3 K when the magnetic field exceeds 5 T, as mentioned in the caption of figure 5.

Figure 6 shows susceptibility measurements  $\chi(T)$ , at magnetic fields from 0.01 T to 5 T. Those results indicated than at a field of 3.5 T, the peak at  $T = 3.3$  K disappears. This change in the magnetic behavior is related with a metamagnetic transition. Thus, the applied field  $\geq 3.5$  T, in this compound, is the critical field at which the constraints of crystal field are exceeded, and the magnetic behavior changes.

These results can be compared with those found in other  $Ni^{2+}$  systems. Evidences of a metamagnetic transition in  $Ni(C_2O_4)(bpy)$  was also obtained in polycrystalline materials [5]. The transition has been anticipated by slope changes in  $M(H)$  with higher applied fields, i.e.,

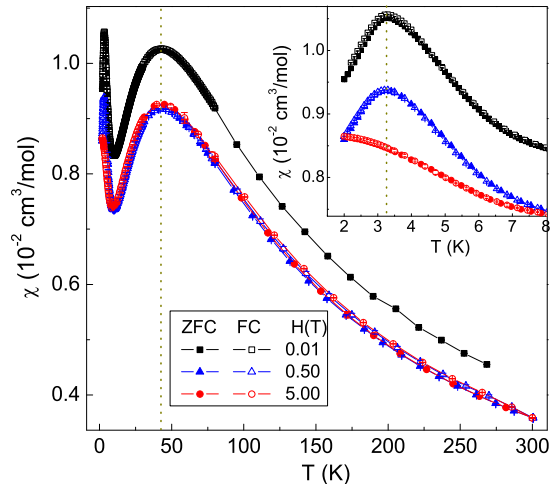


FIG. 5. (Color online) Main panel: molar susceptibility of  $\beta - NiC_2O_4 \cdot 2H_2O$  with maximum at around 43 K, for both ZFC and FC modes, measured with three applied fields: 0.01 T, 0.50 T and 5.00 T. Inset: displays the susceptibility at low temperature. The maximum at about 3.3 K changes and disappears when the applied magnetic field exceeds 5 T.

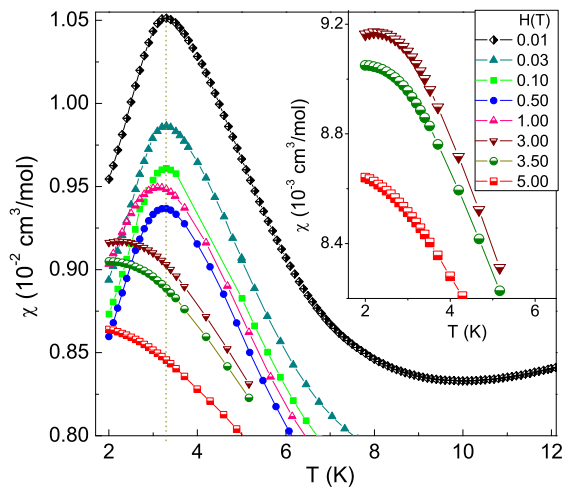


FIG. 6. (Color online) This figure presents in the main panel the Molar susceptibility at low temperature with applied fields from 0.01 to 5.00 T, clearly is seen the evolution of the molar susceptibility with increasing field. The Inset displays three curves measured with magnetic fields from 3 to 5 T. At a field about 3.5 T the maximum at 3.3 K disappears.

$H > 30$  kG and below  $T_N = 26$  K. In this compound, the one-dimensional magnetic character can be enhanced by replacing the transaxial aquo group by organic groups, such as bipyridine. This has the effect of reducing the interchains interaction and consequently the Néel temperature, and the critical fields required for the metamagnetic transitions [19, 20]. Important examples about these behavior are  $CoCl_2 \cdot 2H_2O$ , and  $\alpha - Co(pyridine)_2Cl_2$  [21]. The details of the magnetic properties of these materials are best understood by examining single crystal data because the transitions are sensitive to the orientation of the applied field [1].

It is important to mention that in figure 5, we show that the magnetic susceptibility presents a wide maximum at about 43 K. From 100 K to room temperature  $\chi(T)$  smoothly decreases, and a paramagnetic Curie-Weiss behavior can be fitted. The maximum value at 43 K changes with the magnetic field applied as shown in this figure. The changes are on the range from  $0.91 \times 10^{-2}$  to  $1.03 \times 10^{-2} \text{ cm}^3/\text{mol}$ . This behavior is quite similar to the reported in other compounds, as  $Ni(pip)(C_2O_4)$ , where pip= piperazine, which is formed by chains of  $[Ni(ox)]_n$  and  $[Ni(pip)]_n$ . In that example, a broad maximum is observed and occurs at 53(1) K [22]. So, accordingly the broad maximum in the susceptibility in our compound is a typical behavior of a low dimensional antiferromagnetic system [23].

In figure 7 we show a plot of the inverse of susceptibility,  $\chi(T)^{-1}$  at  $H = 0.01, 0.50$  and  $5.00$  T, for  $\beta - NiC_2O_4 \cdot 2H_2O$ . The analysis of these measurements was performed by fitting a Curie-Weiss from room temperature to 100 K. The fit parameters were Weiss temperature  $\theta_\omega$  and Curie constant  $C$  varying from  $-76.90$  to  $-99.82$  K and from  $1.35$  to  $1.67 \text{ cm}^3 \text{ mol}^{-1} \text{ K}$ , respectively.

The fit parameters could be used to calculate the effective magnetic moment  $\mu_{eff}$  per mole from equation  $\mu_{eff} = 2.84[C]^{1/2} = 2.84[\chi T]^{1/2}$ , which is shown in figure 8.

An important aspect of the behavior  $\mu_{eff}$ , for this compound, and related to Curie constant, and the large negative Weiss constant, is indicative of a significant antiferromagnetic exchange interactions between neighbouring nickel ions, and a big degree of frustration [24]. It is quite possible because the metamagnetic transition obtained in figures 5 and 6. As observed, this dramatic change of the  $\mu_{eff}$  is the effect of the change of the Curie constant, and then via the number of unpaired electrons. Thus, accordingly to  $\mu_{eff} = g[n(n+1)]^{1/2}$ , the number of unpaired electrons  $n$  in  $NiC_2O_4 \cdot 2H_2O$  can be calculated as 1.40, 1.23 and 1.22 respectively for applied field of 0.01 T, 0.50 T and 5.0 T.

In order to understand more about the magnetic characteristics of this oxalate, we studied the  $M - H$  isothermal measurements from the temperature range 2 - 80 K (see figure 9), from these data we extracted the coercive field, which shows a small measurable and perceptible exchange bias. Our measurements of the coercive field, although small, were carefully checked and are below of

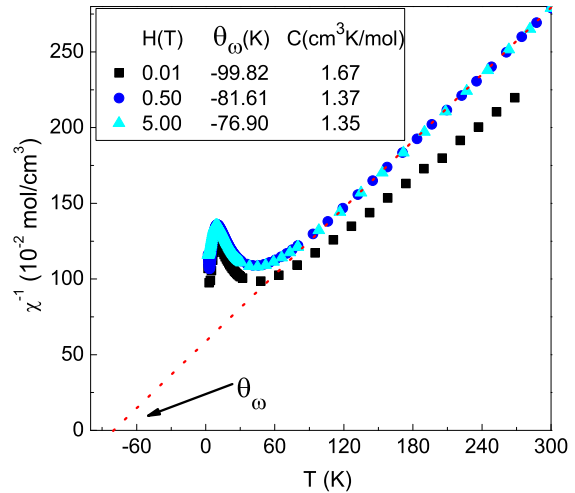


FIG. 7. (Color online) Inverse susceptibility at different magnetic fields,  $\chi^{-1}(T)$  for dihydrate nickel oxalate. The Weiss temperature  $\theta_\omega$ , changes from about  $-76.90$  to  $-99.82$  K. The Curie constant also changes from  $1.35$  to  $1.67 \text{ cm}^3 \text{ mol}^{-1} \text{ K}$ , from high to low magnetic fields.

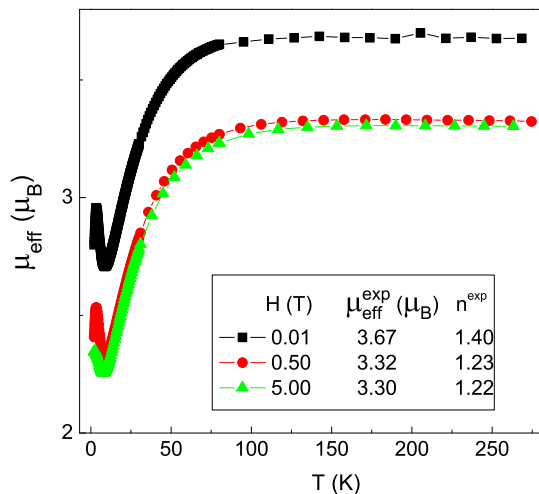


FIG. 8. (Color online) Effective Bohr magneton moments  $\mu_{eff}$  per mol as a function of temperature. At room temperature the values change from  $3.30$  to about  $3.67 \mu_B$ , depending on the magnetic field applied.  $n^{exp}$  is the number of unpaired electrons.

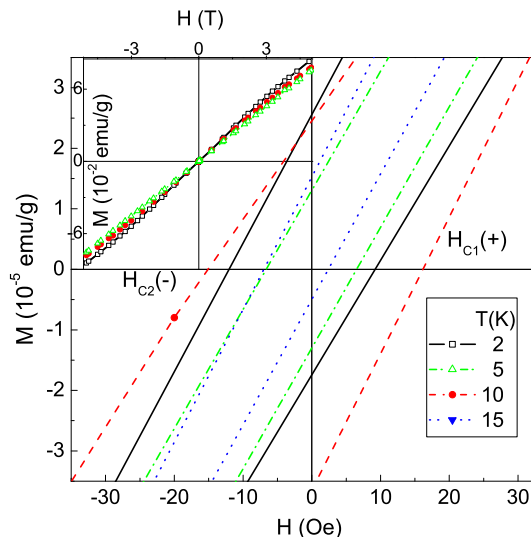


FIG. 9. (Color online) Isothermal magnetization measurements  $M - H$  from 2 to 15 K shown in the main panel. Note the coercive field and the small exchange bias. Inset shows the  $M(H)$  measurements at 4 T and different temperatures from 2 to 80 K. At low fields (main panel) the hysteric effect is clearly observed. The asymmetric behavior in the coercive field is related to a exchange bias effect due to canted spins, but other type of interaction is not discarded as driven by Dzyalochinsky-Moriya type exchange (DM).

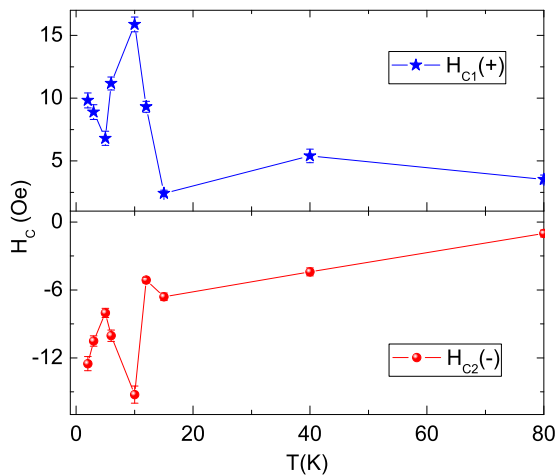


FIG. 10. (Color online) Coercive Field vs Temperature determined by isothermal magnetic measurements.

the possible errors. The results are displayed in figure 10.

This exchange bias can be explained as the effect of inter and intra chains interactions in this compound. The interaction of metallic ions between chains is at the origin of spin canting. This small but measurable exchange bias indicates that instead of produce a pure antiferromagnetic order, the magnetic order has been distorted by canted spins giving rise to weak ferromagnetism. Since weak ferromagnets are a delicate balance of opposing forces, it is not surprising to find that many are also metamagnets [25].

Experimentally, it is important to mention that great care was taken when measuring the exchange bias. Our SQUID magnetometer is provided with a Mu metal shielding. At the moment of performing the magnetization measurements a flux gate magnetometer was used to demagnetize the superconducting coil. This procedure reduces the magnetic field to a very small value to about 0.001 G or less and the Mu shielding eliminates external magnetic influences, as the earth magnetic field.

#### IV. CONCLUSIONS

Microcrystals single phase of orthorhombic nickel (II) oxalate dihydrate were prepared by soft solution chemistry, as observed by XRD powder diffraction. Chemical analysis, DTA and TG studies revealed that the microcrystals are of high purity.  $\chi(T)$  measurements showed the existence of two maxima at 3.3 K and at 43 K. The first one at low temperature changes and disappears with applied magnetic field, this change is due to metamagnetic transition, the maximum disappears with applied field about  $\geq 3.5$  T. The second maximum indicates an antiferromagnetic order, with interactions due to coupled chains via inter- and intrachain interactions and/or DM type-exchange. The effects of interchain interactions disturb the AF coupling, distorting it and canting spins, which in turn produces a weak ferromagnetic order. This WF is evident by hysteresis measurements in M-H isothermal measurements.

#### ACKNOWLEDGMENTS

Partial support for this work is gratefully acknowledge to CONACyT, project No.44296/A-1 and Scholarship CONACyT, register No. 188436 for E. Romero; VIEPBUP, project No. MEAM-EXC10-G. RE, thanks to CONACyT Project 129293(Ciencia Básica), DGAPA-UNAM project No. IN100711, project BISNANO 2011, and project PICCO 11-7 by The Department of Distrito Federal, México.

[1] F. Keffer and H. Chow, Phys. Rev. Lett. **31**, 1061 (1973).

[2] E. R. Jr. Jones and J. A. Stone, J. Chem. Phys. **56**, 1343 (1972).

- [3] T. Liu, Y. Zhang, Z. Wang and S. Gao, *Inorg. Chem.* **45**, 2782 (2006).
- [4] C. M. Hurd, *Contemp. Phys.* **23** (5), 469 (1982).
- [5] T. Yuen, C. L. Lin and T. W. Mihalisin, *J. Appl. Phys.* **87**, 6001 (2000).
- [6] E. Romero, M. E. Mendoza and R. Escudero, *Phys. Status Solidi B* **248**, 1519 (2011).
- [7] R. Deyrieux, C. Berro and A. Péneloux, *Bull. Soc. Chim. Fr.* 25 (1973).
- [8] P. J. Dubernat and H. Pezerat, *J. Appl. Cryst.* **7**, 378 (1974).
- [9] M. Molinier, D. J. Price, P. T. Wood and A. K. Powell, *J. Chem. Soc., Dalton Trans.*, 4061 (1997).
- [10] R. Deyrieux and A. Péneloux, *Bull. Soc. Chim. Fr.*, 2675 (1969).
- [11] C. Drouet, A. Pierre and A. Rousset, *Solid State Ionics* **123**, 25 (1999).
- [12] M. Kurmoo, *Chem. Soc. Rev.* **38**, 1353 (2009).
- [13] S. Vaidya, P. Rastogi, S. Agarwal, S.K. Gupta, T. Ahmad, A.M. Antonelli, K.V. Ramanujachary, S.E. Lofland and K. Ganguli, *J. Phys. Chem. C* **112**, 12610 (2008).
- [14] G. A. Bain and J.F. Berry, *J. Chem. Educ.* **85**, 532 (2008).
- [15] L. B. McCusker, R. B. Von Dreele, D. E. Cox, D. Louër and P. Scardi, *J. Appl. Cryst.* **32**, 36 (1999).
- [16] B. D. Cullity, *Elements of X-Ray Diffraction*, 2nd ed (Reading, Massachusetts: Addison Wesley), 259 (1978).
- [17] D. Zhan, C. Cong, K. Diakite, Y. Tao and K. Zhang, *Thermochim. Acta* **430**, 101 (2005).
- [18] A. N. Zakharov, A. F. Mayorova and N. S. Perov, *J. Therm. Anal. Cal.* **92**, 747 (2008).
- [19] T. Otieno and R. C. Thompson, *Can. J. Chem.* **73**, 275 (1995).
- [20] L. Mao, S. J. Rettig, R. C. Thompson, J. Trotter and S. Xia, *Can. J. Chem.* **74**, 433 (1996).
- [21] S. Foner, R. B. Frankel, W. M. Reiff, H. Wong and G. J. Long, *J. Chem. Phys.* **68**, 4781 (1978).
- [22] T. D. Keene, H. R. Ogilvie, M. B. Hursthouse and D. J. Price, *Eur. J. Inorg. Chem.* **2004**, 1007 (2004).
- [23] J. C. Bonner and M. E. Fisher, *Phys. Rev.* **135**, A640 (1964).
- [24] A. P. Ramirez, *Handbook of Magnetic Materials* (Ed K. H. J. Buschow) **13**, 423 (2001).
- [25] E. Stryjewski and N. Giordano, *Adv. Phys.* **26** (5), 487 (1977).